JACS Au
AN OPEN ACCESS JOURNAL OF THE AMERICAN CHEMICAL SOCIETY

pubs.acs.org/jacsau
Article

Engineering a Metal Reductase for the Bioremediation of Anthropogenic Electronic Wastes: From Hg(II) to Au(III) and Ag(I) Enzymatic Reduction

Published as part of JACS Au virtual special issue "Biocatalysis in Asia and Pacific".

Jasmine Puay Suan Chua,[‖] Rashmi Rajasabhai,[‖] Wei Zhe Teo, Bo Xue, and Wen Shan Yew*

Cite This: *JACS Au* 2024, 4, 2335−2342

Read Online

ACCESS | Metrics & More | Article Recommendations | Supporting Information

ABSTRACT: Recovering precious metals from electronic waste (e-waste) using microbes presents a sustainable methodology that can contribute toward the maintenance of planetary health. To better realize the potential of bioremediation using engineered microbes, enzymes that mediate the reduction of Au(III) to Au(0) have been the subject of intense research. In this study, we report the successful engineering of a metal reductase, MerA, whose cognate substrate is mercury(II), toward other precious metals such as Au(III) and Ag(I). The engineered variant, G415I, exhibited a 15-fold increase in catalytic efficiency (k_{cat}/K_M) in Au(III) reduction to Au(0) and a 200-fold increase in catalytic efficiency in Ag(I) reduction to Ag(0) with respect to the wild-type enzyme. The apparent shift in preference toward noncognate metal ions may be attributed to the energetics of valency preference. The improved Au(III) reductase has an apparent increased preference toward monovalent cations such as Au(I) and Ag(I), with respect to divalent cations such as Hg(II), the cognate substrate of the progenitor MerA (an increase in K_M of 5.0-fold for Hg(II), compared to a decrease in K_M of 5.8-fold for Au(III) and 1.8-fold for Ag(I), respectively). This study further extends the mechanistic understanding of Au(III) bioreduction that could proceed through the stabilization of Au(I) en route to Au(0) and suggests that the biosynthesis of Au nanoparticles with high efficiency can be realized through the engineering of promiscuous metal reductases for precious metal recovery from e-wastes.

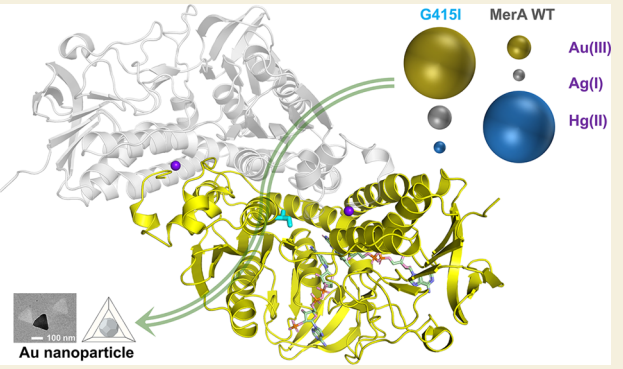

KEYWORDS: *Au(III) reductase, gold nanoparticles biosynthesis, precious metal recovery, enzyme engineering, e-waste, bioremediation*

INTRODUCTION

Advancement in technology, coupled with reduced innovation cycles and rapid development of new electronic devices, contributed to the increase in electronic waste (e-waste) as consumers adopted the use of these devices and changed to newer models more frequently. According to the United Nations, around 53.6 million metric tons of e-waste are produced worldwide yearly,[1,2] and this figure is projected to reach 75 million metric tons by 2030.[2−4] However, of all the e-waste generated, only 17% are recycled,[1] resulting in an ever-increasing accumulation of e-waste and calls for more efficient recycling efforts.

Currently, there are two main steps in e-waste recycling. The first step is preprocessing, and the second step is end-processing. For preprocessing, it involves physical methods to pretreat the e-waste, such as disassembly, shredding, and mechanical separation. End-processing is a process that recovers valuable metals such as gold from the pretreated e-waste. Common end-processing processes are pyrometallurgy and hydrometallurgy.[5] A major drawback in the use of pyrometallurgy and hydrometallurgy methods is the generation of hazardous byproducts which have severe adverse environmental impact.[3] Consequently, the biometallurgy method, which uses microbes to leach out valuable metals such as gold with minimal adverse environmental impact, is gaining popularity as an alternative end-processing technique.[6] However, the method requires improvement in bioleaching rates, microorganism toxicity tolerance, and substrate specificity for widespread commercial application.[5,7]

Electronic products comprise a mixture of different precious metals such as Au, Ag, and Pt.[8,9] For example, a printed circuit board (PCB) is made up of more than 20 types of metals,

Received: April 3, 2024
Revised: May 23, 2024
Accepted: May 24, 2024
Published: May 31, 2024

Table 1. Kinetic Parameters for MerA from *P. aeruginosa*, *B. cereus*, and *A. ferrooxidans* on Different Metal Substrates

enzyme		substrate ions	parameter		
			k_{cat} (s^{-1})	K_M (μM)	k_{cat}/K_M (M^{-1} s^{-1})
MerA	*P. aeruginosa*	**Hg(II)**	15 ± 5.1	96 ± 58	(15 ± 7) × 10^4
		Au(III)	(27 ± 3.0) × 10^{-3}	290 ± 85	91 ± 32
		Ag(I)	(0.25 ± 0.1) × 10^{-3}	460 ± 350	0.54 ± 0.30
		Pd(II)	(0.14 ± 0.06) × 10^{-3}	470 ± 340	0.30 ± 0.17
		Pt(IV)	(0.11 ± 0.01) × 10^{-3}	250 ± 76	0.44 ± 0.18
		Cd(II)	(0.09 ± 0.04) × 10^{-3}	1091 ± 978	(0.79 ± 0.44) × 10^{-1}
	B. cereus	**Cr(III)**	(3.5 ± 0.5) × 10^{-3}	740 ± 200	4.8 ± 2.5
	A. ferrooxidans	**Co(II)**	(2.3 ± 0.9) × 10^{-3}	1800 ± 990	1.3 ± 0.9

including precious metals.[10] The precious metals in e-waste are the major components of interest to be recovered because of their abundance in e-waste, scarcity in natural reserves, and increasing market value.[3,5] However, the complexity of e-waste makes it difficult to develop a processing method to recover all precious metals.[3,11] Hence, it would be advantageous if a microbial host expressing a desired enzyme could participate in the recovery of precious metals of interest from the e-waste. An enzyme is an efficient biocatalyst that lowers the activation energy of a reaction that converts a specific (or at most a few similar types) substrate to a product.[12] In order to achieve the goal of developing an enzyme for the recovery of several different precious metals from e-waste, deliberate efforts would have to be made to obtain an enzyme that is both promiscuous (and thereby increasing the range of precious metal substrates) and efficient (in terms of biocatalytic reduction of X ($N \geq 1$) to X (0) for recovery, where X can be Au, Ag, Pt, etc.). This will involve the engineering of a progenitor enzyme, a metal reductase, that can be catalytically reactive toward several metal ions.

The choice of a progenitor enzyme can be made on the basis of known substrate specificity, such as the selection of a gold reductase[13] as the starting enzyme template and with the expectation of the associated reduction of Au(III) to Au(0). However, the promiscuity of this enzyme on other precious metals was not demonstrated, and it is not as well studied as other metal reductases. Hence, we chose a metal reductase such as mercury reductase MerA, that is well studied and characterized and has been previously shown to exhibit promiscuous reduction activity, as the progenitor.[14] MerA functions as a homodimeric enzyme where its catalytic core has two interfacial active sites.[15] Its physiological catalytic activity is to detoxify and reduce Hg(II) to Hg(0), which will be relatively unreactive and exit cells passively and safely.[15] Previous studies have shown that incubating the cell-free extracts of *P. aeruginosa* with Au(III)-containing solution led to the formation of gold nanoparticles, which has been hypothesized to be attributed to the presence of endogenous MerA enzyme in the extract.[16,17] This suggests that MerA may exhibit promiscuous metal ion-reducing activity toward gold ions and reduce Au(III) to Au(0), generating gold nanoparticles.

Gold nanoparticles are widely used in medical and nonmedical applications, ranging from photothermal cancer therapy, protein labeling to electronic chips,[18,19] making this versatile material to be highly sought after. However, high labor and manufacturing cost of producing gold nanoparticles have driven its price to 450-fold of gold bullion's value.[20] The use of metal reductases on e-waste to recover precious metal gold has the potential to increase the supply of gold nanoparticles in a sustainable manner; hence, there is a distinct economic and environmental advantage in engineering a metal reductase for gold recovery from e-waste.

In this study, we examined MerA's suitability as a metal reductase including the formation of gold nanoparticles from Au(III) ions. We demonstrated the feasibility of engineering a promiscuous MerA for increased preference toward precious metal substrates such as Au(III) and Ag(I). We propose the possible mechanistic implication of the increased catalytic activity of a G415I variant on Au(III). This work also suggests a tractable route in engineering a promiscuous metal reductase for precious metal recovery from e-waste and is an important step toward developing biobased sustainable solutions that can advance biometallurgical recycling of e-waste.

RESULTS AND DISCUSSION

Promiscuity of MerA Variants

E-waste is made up of different materials, and the composition is usually complex. To recover several metals from e-waste using a single enzyme, we examined several MerA orthologues originating from different organisms to determine the range of enzyme−substrate promiscuity. We are interested in identifying a naturally occurring MerA with the highest gold reduction potential and further engineering selected MerA to improve its catalytic activity on selected metal ions. Using MerA from *P. aeruginosa* as a query sequence in enzyme function initiative−enzyme similarity tool (EFI-EST), a sequence similarity network (SSN) was generated.[21] An alignment score threshold of 81, corresponding to approximately 40% sequence identity, was used. Orthologs with 39−95% sequence identity to query sequence, annotated as mercuric reductase A, and have protein-level evidence were selected (Table S1: Protein sequence of MerA and its variant G415I). MerA genes from *P. aeruginosa*, *B. cereus*, and *A. ferrooxidans* (Table S1) were expressed and purified in *E. coli* cells. The activity of each MerA was then tested on 15 different metal substrates that are commonly found in e-waste[22,23] (Figure S1: Reaction schematic of MerA and its variants and list of metal ion substrates tested). Reactions of 50 μL were set up containing 100 mM KH_2PO_4 (pH 7.6), 0.4 mM NADPH, 0.02 mM MerA or other variants, and varying concentrations of metal ions (0.01−1 mM) (Figure S1). Enzyme kinetics were determined by monitoring NADPH oxidation at 340 nm and 25 °C. The rate of NADPH oxidation is directly proportional to the rate of metal ion reduction. Using a nonlinear regression fit to Michaelis−Menten conditions, kinetic parameters were estimated based on the measured initial velocity of NADPH oxidation. Out of the 15 metal ions tested, eight of them were determined to act as substrates for MerA, and the catalytic

https://doi.org/10.1021/jacsau.4c00297
JACS Au 2024, 4, 2335−2342

efficiencies of MerA with respect to each metal ion are shown in Table 1. From the kinetics data obtained, we could surmise that MerA from *P. aeruginosa* is the most promiscuous with activity measured for reduction of six metal ions, including gold ions (Table 1). Husseiny and co-workers have demonstrated that MerA from *P. aeruginosa* could be contributing to the formation of gold nanoparticles when cell-free extracts of *P. aeruginosa* were incubated with Au(III)-containing solution.[16] This corroborates well with our data, as MerA from *P. aeruginosa* has shown the capability of reducing Au(III) ions (Table 1), and gold nanoparticles could be observed under transmission electron microscopy (TEM) (Figure 1A). Furthermore, the formation of a reddish

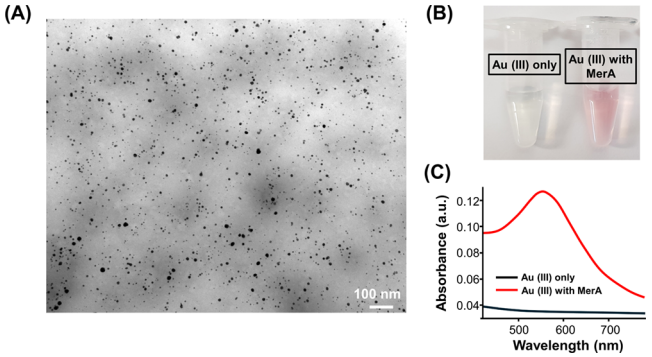

Figure 1. Production of gold nanoparticles using MerA. (A) TEM image of spherical gold nanoparticles obtained from the reduction of Au(III) using MerA. Scale bar represents 100 nm. (B) Picture depicting a reddish solution of gold nanoparticles obtained with MerA. (C) Graph of absorbance against wavelength of the Au(III) solution (black) and Au(III) incubated with MerA (red).

coloration (Figure 1B) and the presence of an absorbance peak at 520 nm upon MerA incubation with Au(III) (Figure 1C) indicated the presence of gold nanoparticles, in accordance with observations in published literature regarding gold nanoparticle formation.[24,25] As MerA from *P. aeruginosa* seems to be promiscuous (Table 1), it would be advantageous to engineer MerA to have increased catalytic efficiency in the reduction of precious metal ions, such as gold ions and silver ions. Hence, we focused our efforts on MerA from *P. aeruginosa* for subsequent experiments.

Directed Evolution of MerA for Increased Au(III) Reduction Activity

With MerA from *P. aeruginosa* as the progenitor template (termed WT MerA), we created a mutant library using the deep scanning mutagenesis method (Figure S2: Deep scanning mutation method in creating a systematic mutant library). A mutant library of 8873 mutants, consisting of 19 mutations for each of the 467 residues, was generated and screened for active variants through directed evolution.[26,27] The directed evolution platform is described in Figure S3 (Schematic of directed evolution of MerA toward increased Au(III) reduction activity), and the top 16 active variants were selected from the screen. These variants were then expressed, purified, and characterized (Figure S4: SDS-PAGE gel analysis of the soluble fraction of MerA WT and its variants).

Kinetic Studies of Selected Variants from the Screen

Kinetic parameters of the mutants' ability to reduce Au(III) ions were determined using a kinetic assay (Figure S1), and the results are shown in Figure 2 and Table S2, while the site of

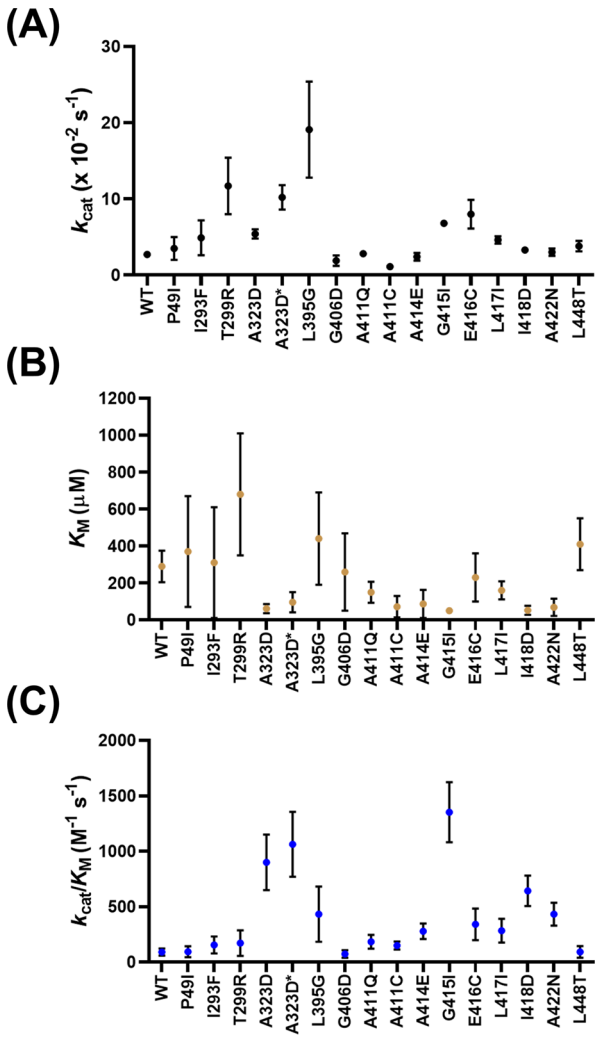

Figure 2. Kinetic parameters of WT MerA and variants on the reduction of Au(III) ions. (A) k_{cat} measurements of WT MerA and its variants. Variant L395G has the highest k_{cat} compared to that of WT MerA. (B) K_M measurements of MerA and variants. Several variants such as A323D, A323D*, A411C, A414E, G415I, I418D, and A422N have one of the lowest K_M. (C) k_{cat}/K_M values of WT MerA and variants. Variant G415I has the greatest improvement in catalytic efficiency as compared to WT MerA.

mutation (residue number) for the 16 variants is indicated in Figure S5 (Mutations and their positions on MerA variants). All of the variants bear a single substitution mutation, except for variant A323D*, which has an additional deletion of 42 residues immediately downstream of the A323D substitution; two of the selected variants have mutations occurring at residue number 411. The kinetic parameters indicated that variant G415I has the most improved catalytic efficiency on Au(III) ions as compared to WT MerA (15-fold improvement); other variants with significant improvement in their catalytic activities include A323D* (A323D and del324−365, 12-fold), A323D (10-fold), I418D (7-fold), L395G (5-fold), and A422N (5-fold), which all involve hydrophobic amino acids, with their side chains being either truncated or changed to polar or negatively charged ones. When visualized based on the PDB structure of MerA (PDB 4K7Z), it becomes apparent that the mutated residues (except for the 42-residue deletion) do not directly interact with the bound FAD, NADP, or metal ion (Hg in this case) (Figure 3). The G415I mutation is

https://doi.org/10.1021/jacsau.4c00297
JACS Au 2024, 4, 2335−2342

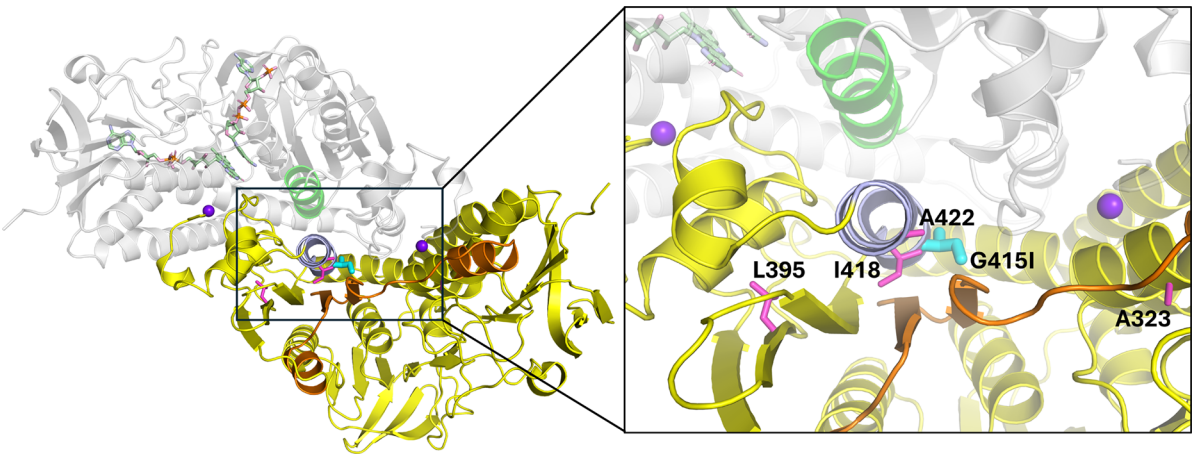

Figure 3. Positional elements in MerA that enhance Au(III) reduction. The locations of the beneficial mutations on MerA are depicted. The two MerA monomers in the dimer are shown as ribbons and colored yellow and gray, respectively. The 42-residue deletion in variant A323D* is colored orange. Side chains of beneficial mutations are shown as sticks and are labeled in the enlarged view. The WT side chains to be mutated are colored magenta, and the introduced side chain of isoleucine in variant G415I is colored cyan. Bound FAD and NADP are colored green and shown as sticks on only one monomer for clarity. Bound Hg(II) atoms are shown as spheres and colored purple. The interfacial helices (residues 413−427) harboring the greatest number of beneficial mutations are highlighted in light blue and light green, respectively.

Table 2. Kinetic Studies of WT MerA and Variant G415I on Different Metal Ions

		kinetic parameters		
substrate ions	MerA enzyme	k_{cat} (s^{-1})	K_M (μM)	k_{cat}/K_M (M^{-1} s^{-1})
Hg(II)	WT	15 ± 5.10	96 ± 58	(15 ± 7) × 10^4
	G415I	(14 ± 0.06) × 10^{-3}	470 ± 340	30 ± 1.7
Au(III)	WT	(27 ± 3) × 10^{-3}	290 ± 85	(0.91 ± 0.32) × 10^2
	G415I	(6.8 ± 0.3) × 10^{-2}	50 ± 11	(1.35 ± 0.27) × 10^3
Ag(I)	WT	(0.25 ± 0.1) × 10^{-3}	460 ± 350	0.54 ± 0.3
	G415I	(2.9 ± 0.3) × 10^{-2}	260 ± 45	110 ± 1.2

located at the dimer interface of MerA, on an α-helix that faces its symmetrical counterpart in the MerA dimer; the introduction of the bulkier isoleucine side chain at this position is, therefore, likely to alter the conformation of this α-helix, which, in turn, leads to modified catalysis at the dimer interface (see below). The I418D and A422N mutations are at the back of the same α-helix in a largely hydrophobic environment; analogous to G415I, introducing charged or polar residues at these positions is expected to have impacted the conformation of the α-helix and MerA activity. Similar to I418D and A422N, the A323D mutation is also at the back of another interfacial α-helix in the FAD/NADP binding domain and is located in a region surrounded by hydrophobic residues.

The only beneficial mutation away from the MerA dimer interface, L395G, is at the hydrophobic core of the reductase dimerization domain, which could have significant allosteric influence propagating from the domain to the dimer interface. Lastly, the simultaneous substitution and deletion observed in A323D* will undoubtedly alter the intramolecular packing between the FAD/NADP binding domain and the reductase dimerization domain, which in turn will change or even abolish intermolecular interactions between two MerA molecules. Taken together, an alteration in the dimer interfacial interaction of MerA seems to be the main reason for the observed enhanced activity in the reduction of metal ions by engineered variants.

To examine the impact of the G415I mutation on the dimerization of MerA molecules, size-exclusion chromatography (SEC) coupled with multiangle light scattering (MALS) was adopted to analyze purified proteins of WT MerA and the G415I variant. The data obtained from SEC-MALS suggest that the G415I mutation does not cause significant changes to the stability of MerA dimers (Figure S6). The eluted dimer peaks of WT MerA and the G415I variant from SEC show minimal differences in their retention volume and estimated mass by MALS (106.8 kDa for the WT vs 107.2 kDa for the G415I variant). To probe subtle structural alterations introduced by the beneficial mutations, molecular dynamics simulations were conducted, and the centers-of-mass of the two interfacial α-helices were measured (Figure 3 and Table S3: Averaged distances between MerA interfacial helices over 1 ns molecular dynamics simulations). From the measured average distances of 3 independent, 1 ns simulations for each variant, small but reproducible increases in the distance can be clearly observed for G415I and I418D. Collectively, the beneficial G415I mutation seems to alter MerA's activity by fine-tuning local interactions without causing global disruptions at the dimer interface. We postulate that similar effects could be exerted by the other beneficial mutations.

The effect of subtle conformational changes at the dimer interface on the catalytic activity and substrate preference of MerA can be understood from the cooperativity of the two MerA molecules during catalysis. Specifically, the C-terminal cysteine pair of one MerA molecule would capture the substrate ion, mercury, for example, and pass it through the dimer interface to the N-terminal cysteine pair of the other MerA molecule, as proposed by Ledwidge et al.[15] Consequently, small conformational changes at the dimer interface,

https://doi.org/10.1021/jacsau.4c00297
JACS Au 2024, 4, 2335−2342

which translate to modest perturbations to the association of the dimer, could significantly impact upon the distances and geometries of MerA's interfacial active site. In the case of the beneficial mutations, such changes led to dramatically reduced activity of MerA toward its cognate substrate Hg(II) ions, while resulting in enhanced activities toward Au(III) ions and Ag(I) ions, respectively. While the former (reduction of Hg(II) ions) may be tractably comprehended, the latter (reduction of Au(III) ions and Ag(I) ions) is more elusive and awaits further investigations. It is worth noting that this interfacial active site of MerA is not an ubiquitous feature among metal reductases: as an example, the reported Au(III) reductase from *Erwinia* sp. IMH, despite being a homodimer like MerA, catalyzes Au(III) ion reduction within each active site of the monomer without the involvement of interfacial interactions.[13]

Kinetic Studies of WT MerA and Variant G415I on Selected Metal Ions

Kinetic studies of WT MerA and variant G415I on reduction of Hg(II) ions, Au(III) ions, and Ag(I) ions were carried out, and the values obtained are shown in Table 2. It was observed that variant G415I has lower catalytic efficiency for the reduction of Hg(II) ions by about 4 orders of magnitude as compared to WT MerA. On the other hand, variant G415I has demonstrated improved catalytic efficiencies by one and two orders of magnitude as compared to WT MerA for the reduction of Au(III) ions and Ag(I) ions, respectively.

A single mutation in variant G415I has altered MerA's activity: the engineering of MerA has reduced its substrate specificity on its natural substrate Hg(II) ions and improved catalytic efficiency on the reduction of Au(III) ions and Ag(I) ions. For future work, we could explore combining other mutations identified in other MerA variants with variant G415I to find out if there is any synergistic effect toward improving MerA's catalytic efficiency on the reduction of Au(III) ions and Ag(I) ions.

As the reduction of metal ions by MerA variants requires the cofactor NADPH, it would be more cost efficient if we could couple this reaction to a NADPH regeneration system. Enzymes such as phosphite dehydrogenase[28] could be expressed in a single plasmid with genes expressing MerA variants to provide NADPH regeneration for the metal reduction reaction performed by MerA variants.

TEM Analysis of Gold Nanoparticles (AuNP)

To further delineate the reduction activity of MerA variant G415I on Au(III) ions, *E. coli* cells expressing variant G415I were separately incubated with Au(III) ion-containing solution and preprocessed e-waste leachate, respectively. The samples were analyzed using TEM. Gold nanoparticles of about 100 nm were observed for both substrate solutions (Figure 4). The shape of the gold nanoparticle observed is a truncated tetrahedron that could have developed from a single-crystalline gold nanoparticle seed. This corroborates well with a previous study by Langille et al., where images of products of the same reaction were shown to have different particle morphologies, ranging from pseudospherical seed to icosahedron.[29] This preliminary data support the potential application of engineered MerA variants on gold recovery and, in particular, the biomanufacturing of gold nanoparticles from e-waste.

Mechanistic Implications on Au(III) Bioreduction

When visualized based on the PDB structure of MerA (PDB entry 4K7Z), it becomes apparent that all the beneficial

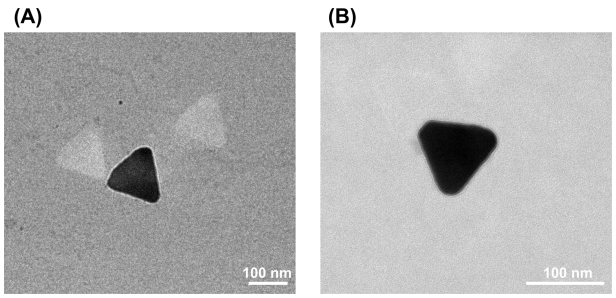

Figure 4. TEM images of the gold nanoparticles. Gold nanoparticles produced by reduction of Au(III) using MerA variant G415I with (A) Au(III) ion-containing solution and (B) e-waste leachate. Scale bars represent 100 nm.

mutations are located near the MerA dimer interface; the single substitutions and the additional deletion in A323D (delΔ324−365) all seem to modulate the interfacial active site of MerA. This altered active site may cause the MerA variants to have increased preference toward monovalent cations such as Au(I) ions and Ag(I) ions with respect to divalent cations such as Hg(II) ions (Table 2). Indeed, variant G415I has clearly demonstrated the shift in its valency preference with concerted improvements for both Au(I) ions and Ag(I) ions reduction. As Au(I) ions are the most stable form of Au(N) ions, vis-à-vis Au(III), the apparent shift in binding preference toward monovalent cations for variant G415I, as with the observed increase in gold reduction, can also be attributed to the energetics of valency preference. In our experiments, we used Au(III) ions as the substrate for our enzymatic gold ion reduction, and this presumably suggests that a possible Au(III) ion reduction mechanism could proceed as such: from Au(III) to Au(I) to Au(0).

In conclusion, we have demonstrated that engineering a promiscuous metal reductase, MerA, toward Au(III) ions has shifted its substrate preference away from Hg(II) ions. Variant G415I has shown a decrease in catalytic activity for the reduction of Hg(II) ions (5000-fold decrease) and an increase in catalytic activity for the reduction of Au(III) ions (15-fold increase) and Ag(I) ions (200-fold increase), with the highest catalytic activity on Au(III) among the three metal substrates. This observation suggests that the G415I mutation, which is located at the dimer interface of MerA, might have altered the dimer formation and brought about a possible increase in the preference for monovalent cations. This study serves as a primer for efforts in engineering efficient metal reductases for precious metal recovery from e-waste. There is the expectation that future work can be expanded toward improvements in biometallurgy metal recovery technologies.

MATERIALS AND METHODS

Strains, Reagents, and Metal Substrates

Cadmium chloride ($CdCl_2$), chromium(III) chloride hexahydrate ($CrCl_3 \cdot 6H_2O$), chromium(VI) oxide (CrO_3), cobalt(II) chloride hexahydrate ($CoCl_2 \cdot 6H_2O$), copper(II) sulfate pentahydrate ($CuSO_4 \cdot 5H_2O$), gold(III) chloride ($AuCl_3$), iron chloride ($FeCl_3$), manganese(II) chloride tetrahydrate ($MnCl_2 \cdot 4H_2O$), mercury(II) chloride ($HgCl_2$), nickel(II) chloride hexahydrate ($NiCl_2 \cdot 6H_2O$), palladium(II) chloride ($PdCl_2$), platinum(IV) chloride ($PtCl_4$), potassium tetrachloroplatinate (II) (K_2PtCl_4), silver nitrate ($AgNO_3$), and zinc chloride ($ZnCl_2$) were obtained from Sigma-Aldrich Co. (St. Louis, Missouri, USA). Reduced β-nicotinamide adenine dinucleotide phosphate (NADPH), L-arabinose, ampicillin,

https://doi.org/10.1021/jacsau.4c00297
JACS Au 2024, 4, 2335−2342

and kanamycin were purchased from Merck (Darmstadt, Germany). Isopropyl β-D-1-thiogalactopyranoside (IPTG) was purchased from Invitrogen (Waltham, Massachusetts, USA). MerA protein sequences from *P. aeruginosa* (PDB 1ZK7), *B. cereus* (Uniprot P16171), and *A. ferrooxidans* (Uniprot P17239) were synthesized, codon optimized for *E. coli* expression (Integrated DNA Technologies, USA) (Table S1).

Cloning of MerA and Its Variants

The MerA sequence from *P. aeruginosa* (PDB 1ZK7), *B. cereus* (Uniprot P16171), and *A. ferrooxidans* (Uniprot P17239) was cloned into a pET-20b vector with the addition of an N-terminal 6× His-Tag sequence and a stop codon. Plasmid containing the MerA gene was transformed into *E. coli* BL21(DE3) for protein expression.

Protein Expression and Purification

The *E. coli* cells carrying the respective plasmid were grown in LB at 37 °C, supplemented with 100 μg/mL ampicillin. When the optical density (OD) at 600 nm reached 0.4, the cells were induced with 0.1 mM IPTG and incubated at 16 °C for 18 h for protein expression. The cells were harvested by centrifugation, and the cell pellet was resuspended in binding buffer (20 mM Tris−HCl (pH 8.0), 500 mM NaCl, 5 mM imidazole). Lysis was performed via sonication. The lysate was subjected to centrifugation at 15,000 rpm for 30 min. The supernatant was collected and loaded onto a chelating Sepharose resin (GE Healthcare Bio-Sciences Corp) charged with Ni^{2+} ions. The column was washed with five column volumes (CV) of binding buffer, followed by five CV of wash buffer (20 mM Tris, pH 8.0, 500 mM NaCl, and 107 mM imidazole). Lastly, the protein was eluted with five CV of elute buffer (20 mM Tris−HCl (pH 8.0), 500 mM NaCl, and 100 mM L-histidine). Fractions containing the recombinant proteins were pooled and dialyzed with 20 mM EDTA to remove Ni^{2+} ions, followed by storage buffer (20 mM KH_2PO_4 (pH 7.6), 100 mM NaCl).

SDS-PAGE Gel Analysis

The *E. coli* cells carrying the WT MerA and the 16 variants' plasmids were grown in LB at 37 °C, supplemented with 100 μg/mL ampicillin. The cells were induced with 0.1 mM IPTG when the OD at 600 nm reached 0.8. They were incubated at 16 °C for 18 h for protein expression. The cells were harvested by centrifugation, and the cell pellet was resuspended in binding buffer. Lysis was performed via sonication. The lysate was subjected to centrifugation at 10,000 rpm for 15 min. The supernatant was collected, and an equal volume of 2× SDS loading dye (2× Laemmli sample buffer, 5% v/v β-mercaptoethanol) was added before heating at 95 °C for 5 min. The samples were loaded and ran on 10% SDS-PAGE gel (180 V, 50 min) and stained with Coomassie blue before visualizing on the ChemiDoc MP Imaging System (Biorad, USA).

Size-Exclusion Chromatography−Multiangle Light Scattering (SEC-MALS) Analysis

Superdex 200 Increase 10/300 GL column on an AKTA pure system (Cytiva, USA) was used for SEC analysis. This system is coupled to the DAWN8 and Optilab system for MALS analysis (Wyatt Technology, USA). Equilibration of the column at a constant flow rate of 0.5 mL/min using running buffer (500 mM NaCl, 20 mM Tris−HCl pH 7.9) was first performed. Purified WT MerA was loaded onto the column via a 100 μL sample loop. The same experimental procedure was applied to purified variant G415I proteins. Data was recorded by ASTRA software (Cytiva, USA) and processed.

Molecular Dynamics Simulations of MerA Dimers

MerA dimers were generated by first applying the crystallographic symmetry of the PDB structure of MerA (PDB 4K7Z) to form a dimer, followed by mutating the corresponding residues of the dimer in Pymol[30] to create variant structures each carrying one beneficial point mutation. YASARA[31] was employed to perform three independent, 1 ns molecular dynamics simulations for each of the MerA dimers and to analyze the simulation results.

Promiscuity of MerA and Kinetic Studies of MerA and Its Variants

Reactions were set up containing 100 mM KH_2PO_4 (pH 7.6), 0.02 mM MerA or other variants, 0.4 mM NADPH and varying concentrations of metal ions such as Hg(II), Au(III), or Ag(I) (0.01−1 mM) (Figure S1), with a final reaction volume of 50 μL. Kinetic parameters of the enzymes were determined by monitoring the oxidation of NADPH (ε = 6220 M^{-1} cm^{-1}) at 340 nm at 25 °C. The rate of NADPH oxidation is directly proportional to the rate of metal ion reduction. The initial velocity was measured, and the kinetic parameters were estimated using a nonlinear regression fit (GraphPad Prism software) to Michaelis−Menten conditions. This assay is adopted from previous studies with some modifications.[15]

TEM Analysis of Gold Nanoparticles (AuNP)

0.1 g portion of e-waste (Cimelia Resources Recovery Pte Ltd., Singapore) was dissolved in 10 mL of solution (52.5% nitric acid, 1.5 M hydrochloric acid) in a 50 mL glass bottle for 5 min. 2.5 times v/v of water was added and filtered through a syringe filter with a 0.22 μm membrane. The filtered solution, 5 mL, was incubated with *E. coli* cells expressing MerA variant G415I for 48 h. Solution containing 2.5 μM Au(III) ions was also filtered and incubated with *E. coli* cells expressing MerA variant G415I. The mixture was centrifuged, and the pellet was incubated with 2 mL of 5 M hydrochloric acid on a shaker for 5 min. The solution was centrifuged, and the pellet was incubated with 4 mL of water for 5 min. The mixture was centrifuged, and the supernatant was taken for TEM analysis. The average particle size and morphology of the gold nanoparticles formed were observed by TEM using a JEOL microscope (JEM-1010) with an accelerating voltage of 100 kV. The samples, each 50 μL, were placed on a 400-mesh carbon-coated copper grid at room temperature and dried for an hour.

Deep Scanning Mutagenesis

With the progenitor template MerA from *P. aeruginosa* (wild-type MerA, and henceforth referred to as WT MerA), a mutant library was created using a deep scanning mutagenesis method with Agilent's QuikChange HT Protein Engineering System kit (Agilent, USA). It has an eArray design system called Quikscan-19 which was used to design 10 custom oligonucleotide libraries, with each library targeting a different 150 nucleotide region in the WT MerA gene. This method systematically replaces every amino acid residue at each position of the protein sequence with the other 19 amino acid residues, resulting in 19 mutagenic oligos for each amino acid position (Figure S2). A mutant library consisting of 8873 mutants was generated from WT MerA, which consisted of 467 residues and were screened for active variants.

Directed Evolution of MerA Variants with Increased Au(III) Reduction Activity

The mutant library was transformed into SPG *E. coli* competent cells. The cells were recovered in LB media containing 50 μM Au(III) for 1 h at 37 °C before plating onto agar plates supplemented with 0.02% L-arabinose, 100 μM Au(III) in Tris minimal media, and 100 μg/mL ampicillin. The transformants from each library were then replicated onto new plates that contained higher concentrations of Au(III) ions until less than 10 mutants per library survived. Concentrations of Au(III) ions used in agar plates were 150, 200, and 250 μM. The transformants that survived the higher concentrations of Au(III) ions were individually inoculated into LB media containing 0.02% L-arabinose and 250 μM Au(III) ions. The mutants that survived would be selected as the top potential variants as they are capable of potentially reducing Au(III) ions and counter high Au(III) ion toxicity (Figure S3). This selection assumes that improved survival is based solely on the improved gold reduction capabilities of MerA variants, thereby reducing the toxicity pressure on the cell and allowing for better survival.

https://doi.org/10.1021/jacsau.4c00297
JACS Au 2024, 4, 2335−2342

■ ASSOCIATED CONTENT

Supporting Information

The Supporting Information is available free of charge at https://pubs.acs.org/doi/10.1021/jacsau.4c00297.

Additional experimental details, materials and methods, and results including kinetic parameters, SDS-PAGE gel analysis, SEC-MALS analysis of engineered variants, and averaged distances between MerA interfacial helices over 1 ns molecular dynamics simulations (PDF)

■ AUTHOR INFORMATION

Corresponding Author

Wen Shan Yew − *Department of Biochemistry, Yong Loo Lin School of Medicine, National University of Singapore (NUS), Singapore 117597, Singapore; NUS Synthetic Biology for Clinical and Technological Innovation, Singapore 117456, Singapore; Synthetic Biology Translational Research Programme, Yong Loo Lin School of Medicine, National University of Singapore, Singapore 117599, Singapore;* orcid.org/0000-0002-3021-0469; Phone: (+65) 6516-8624; Email: wenshanyew@nus.edu.sg

Authors

Jasmine Puay Suan Chua − *Department of Biochemistry, Yong Loo Lin School of Medicine, National University of Singapore (NUS), Singapore 117597, Singapore; NUS Synthetic Biology for Clinical and Technological Innovation, Singapore 117456, Singapore; Synthetic Biology Translational Research Programme, Yong Loo Lin School of Medicine, National University of Singapore, Singapore 117599, Singapore*

Rashmi Rajasabhai − *Department of Biochemistry, Yong Loo Lin School of Medicine, National University of Singapore (NUS), Singapore 117597, Singapore; NUS Synthetic Biology for Clinical and Technological Innovation, Singapore 117456, Singapore*

Wei Zhe Teo − *Department of Biochemistry, Yong Loo Lin School of Medicine, National University of Singapore (NUS), Singapore 117597, Singapore; NUS Synthetic Biology for Clinical and Technological Innovation, Singapore 117456, Singapore; Synthetic Biology Translational Research Programme, Yong Loo Lin School of Medicine, National University of Singapore, Singapore 117599, Singapore*

Bo Xue − *Department of Biochemistry, Yong Loo Lin School of Medicine, National University of Singapore (NUS), Singapore 117597, Singapore; NUS Synthetic Biology for Clinical and Technological Innovation, Singapore 117456, Singapore; Synthetic Biology Translational Research Programme, Yong Loo Lin School of Medicine, National University of Singapore, Singapore 117599, Singapore;* orcid.org/0000-0002-5172-2519

Complete contact information is available at: https://pubs.acs.org/10.1021/jacsau.4c00297

Author Contributions

[‖]J.P.S.C. and R.R. contributed equally to this work. CRediT: **Jasmine Puay Suan Chua** data curation, formal analysis, investigation, writing-original draft, writing-review & editing; **Rashmi Rajasabhai** investigation, writing-original draft, writing-review & editing; **Wei Zhe Teo** formal analysis, investigation, methodology, writing-original draft, writing-review & editing; **Bo Xue** data curation, investigation, methodology, project administration, writing-original draft, writing-review & editing; **Wen Shan Yew** conceptualization, funding acquisition, methodology, project administration, resources, supervision, writing-original draft, writing-review & editing.

Notes

The authors declare no competing financial interest.

■ ACKNOWLEDGMENTS

We acknowledge the funding support from the Agency for Science, Technology, and Research of its Industry Alignment Fund-Industry Collaboration Project (IAF-ICP) Grant No. I2001E0068 (B.X. and W.S.Y.).

■ ABBREVIATIONS

Ag, silver; Ag(I), silver(I) ions; Au, gold; Au(0), gold with oxidation state 0; Au(I), gold(I) ions; Au(III), gold(III) ions; AuNP, gold nanoparticles; Cd(II), cadmium(II) ions; Co(II), cobalt(II) ions; Cr(III), chromium(III) ions; E-waste, electronic waste; FAD, flavin adenine dinucleotide; Hg, mercury; Hg(0), mercury with oxidation state 0; Hg(II), mercury(II) ions; K_{cat}, catalytic constant; K_M, Michaelis constant; K_{cat}/K_M, specificity constant; MerA, mercury reductase A; NADP, nicotinamide adenine dinucleotide phosphate; PCB, printed circuit board; PDB, protein data bank; Pd(II), palladium(II) ions; Pt, platinum; Pt(IV), platinum(IV) ions; TEM, transmission electron microscopy; WT, wild-type

■ REFERENCES

(1) Smieja, J.; World Economic Forum. *The enormous opportunity of e-waste recycling*; Circular Economy, 2023. Available from: https://www.weforum.org/agenda/2023/03/the-enormous-opportunity-of-e-waste-recycling/ (accessed March 27, 2023).

(2) Han, P.; Teo, W. Z.; Yew, W. S. Biologically engineered microbes for bioremediation of electronic waste: Wayposts, challenges and future directions. *Eng. Biol.* **2022**, *6* (1), 23−34.

(3) Do, M. H.; Giang, T. N.; Ut, D. T.; Yunho, L.; Trung, H. B. Advances in hydrometallurgical approaches for gold recovery from E-waste: A comprehensive review and perspectives. *Miner. Eng.* **2023**, *191*, 107977−107993.

(4) Nithya, R.; Sivasankari, C.; Thirunavukkarasu, A. Electronic waste generation, regulation and metal recovery: a review. *Environ. Chem. Lett.* **2020**, *19* (2), 1347−1368.

(5) Kumar, A.; Holuszko, M.; Espinosa, D. C. Romano E-waste: An overview on generation, collection, legislation and recycling practices. *Resour., Conserv. Recycl.* **2017**, *122*, 32−42.

(6) Bosecker, K. Bioleaching Metal solubilization by microorganisms. *FEMS Microbiol. Rev.* **1997**, *20*, 591−604.

(7) Habibi, A.; Shamshiri Kourdestani, S.; Hadadi, M. Biohydrometallurgy as an environmentally friendly approach in metals recovery from electrical waste: A review. *Waste Manag Res.* **2020**, *38* (3), 232−244.

(8) Islam, A.; Ahmed, T.; Rabiul, A. M.; Aminur, R.; Monira, S.; Abd, A. A.; Uddin, M. M.; Hwa, T. S.; Mehedi, H. Advances in sustainable approaches to recover metals from e-waste-A review. *J. Cleaner Prod.* **2020**, *244*, 118815−118835.

(9) Magoda, K.; Lukhanyo, M. Biohydrometallurgical Recovery of Metals from Waste Electronic Equipment: Current Status and Proposed Process. *Recycling* **2022**, *7* (5), 67−81.

(10) de Oliveira Camila, M.; Rossana, B.; Alice, T.; Paola, M. Study of Metal Recovery from Printed Circuit Boards by Physical-Mechanical Treatment Processes. In *International Conference on Raw Materials and Circular Economy*, 2022; pp 121−128.

(11) Liu, K.; Tan, Q.; Yu, J.; Wang, M. A global perspective on e-waste recycling. *Circ. Econ.* **2023**, *2* (1), No. 100028.
(12) Robinson, P. K. Enzymes: principles and biotechnological applications. *Essays Biochem* **2015**, *59*, 1−41.
(13) Wang, L.; Yan, L.; Ye, L.; Chen, J.; Li, Y.; Zhang, Q.; Jing, C. Identification and Characterization of a Au(III) Reductase from Erwinia sp. *IMH. JACS Au* **2022**, *2* (6), 1435−1442.
(14) Summers, A. O.; Sugarman, L. I. Cell-free mercury (II)-Reducing activity in a plasmid-bearing strain of Escherichia coli. *J. Bacteriol.* **1974**, *119*, 242−249.
(15) Ledwidge, R.; Patel, B.; Dong, A.; Fiedler, D.; Falkowski, M.; Zelikova, J.; Summers, A. O.; Pai, E. F.; Miller, S. M. NmerA the metal binding domain of mercuric ion reductase removes Hg2+ from proteins, delivers it to the catalytic core, and protects cells under glutathione-depleted conditions. *Biochemistry* **2005**, *44* (34), 11402−11416.
(16) Husseiny, M. I.; El-Aziz, M. A.; Badr, Y.; Mahmoud, M. A. Biosynthesis of gold nanoparticles using Pseudomonas aeruginosa. *Spectrochim Acta A Mol. Biomol Spectrosc* **2007**, *67* (3−4), 1003−1006.
(17) Sahlman, L.; Lambeir, A. M.; Lindskog, S.; Dunford, H. B. The reaction between NADPH and mercuric reductase from Pseudomonas aeruginosa. *J. Biol. Chem.* **1984**, *259* (20), 12403−12408.
(18) Hammami, I.; Alabdallah, N. M.; Al, J. A.; Madiha, K. Gold nanoparticles: Synthesis properties and applications. *J. King Saud Univ. - Sci.* **2021**, *33* (7), No. 101560.
(19) Homberger, M.; Simon, U. On the application potential of gold nanoparticles in nanoelectronics and biomedicine. *Philos. Trans. R. Soc., A* **2010**, *368* (1915), 1405−1453.
(20) Jendrzej, S.; Gokce, B.; Epple, M.; Barcikowski, S. How Size Determines the Value of Gold: Economic Aspects of Wet Chemical and Laser-Based Metal Colloid Synthesis. *ChemPhysChem* **2017**, *18* (9), 1012−1019.
(21) Gerlt, J. A.; Bouvier, J. T.; Davidson, D. B.; Imker, H. J.; Sadkhin, B.; Slater, D. R.; Whalen, K. L. Enzyme Function Initiative-Enzyme Similarity Tool (EFI-EST): A web tool for generating protein sequence similarity networks. *Biochim. Biophys. Acta* **2015**, *1854* (8), 1019−1037.
(22) Cayumil, R.; Khanna, R.; Rajarao, R.; Mukherjee, P. S.; Sahajwalla, V. Concentration of precious metals during their recovery from electronic waste. *Waste Manag* **2016**, *57*, 121−130.
(23) Chakraborty, S. C.; Qamruzzaman, M.; Zaman, M. W. U.; Alam, M. M.; Delowar, H. M.; Pramanik, B. K.; Nguyen, L. N.; Nghiem, L. D.; Ahmed, M. F.; Zhou, J. L.; Mondal Md Ibrahim, H.; Hossain, M. A.; Johir, M. A. H.; Ahmed, M. B.; Sithi, J. A.; Zargar, M.; Ali, M. M. Metals in e-waste: Occurrence, fate, impacts and remediation technologies. *Process Saf. Environ. Prot.* **2022**, *162*, 230−252.
(24) Thanh, N. T.; Maclean, N.; Mahiddine, S. Mechanisms of nucleation and growth of nanoparticles in solution. *Chem. Rev.* **2014**, *114* (15), 7610−7630.
(25) He, X.; Liu, H.; Li, Y.; Wang, S.; Li, Y.; Wang, N.; Xiao, J.; Xu, X.; Zhu, D. Gold Nanoparticle-Based Fluorometric and Colorimetric Sensing of Copper(II) Ions. *Adv. Mater.* **2005**, *17* (23), 2811−2815.
(26) Chen, K.; Arnold, F. H. Tuning the activity of an enzyme for unusual environments: Sequential random mutagenesis of subtilisin E for catalysis in dimethylformamide. *Proc. Natl. Acad. Sci. U. S. A.* **1993**, *90* (12), 5618−5622.
(27) Arnold, F. H. Directed Evolution: Bringing New Chemistry to Life. *Angew. Chem., Int. Ed. Engl.* **2018**, *57* (16), 4143−4148.
(28) Relyea, H. A.; van der Donk, W. A. Mechanism and applications of phosphite dehydrogenase. *Bioorg Chem.* **2005**, *33* (3), 171−189.
(29) Langille, M. R.; Zhang, J.; Personick, M. L.; Li, S.; Mirkin, C. A. Stepwise evolution of spherical seeds into 20-fold twinned icosahedra. *Science* **2012**, *337* (6097), 954−957.
(30) *The PyMOL Molecular Graphics System, Version 2.5.0*; Schrödinger, LLC.
(31) Land, H.; Humble, M. S. In *Protein Egineering*, Bornscheuer; Höhne, Eds.; YASARA: A tool to obtain structural guidance in biocatalytic investigations; Humana Press: New York, NY, 2018; Vol. *1685*, pp 43−67.

https://doi.org/10.1021/jacsau.4c00297
JACS Au 2024, 4, 2335−2342